Communication

Restoration Mechanisms During the Friction Stir Processing of Aluminum Alloys

NARESH NADAMMAL, SATISH V. KAILAS, JERZY SZPUNAR, and SATYAM SUWAS

In the current study, correlation of microstructure evolution with bulk crystallographic texture formation during friction stir processing (FSP) of commercial aluminum alloys has been attempted. Electron backscattered diffraction and X-ray diffraction techniques were employed for characterizing the nugget zone of optimum friction stir processed samples. Volume fraction of measured texture components revealed that the texture formation in aluminum alloys is similar irrespective of the alloy composition. Recrystallization behavior during FSP was more of a composition dependent phenomenon.

DOI: 10.1007/s11661-015-2902-8

Aluminum alloys with copper and magnesium as the major alloying elements are widely used in structural applications due to their high strength to weight ratio and good corrosion resistance.[1] Friction stir processing is a severe plastic deformation (SPD) technique, introduced by Mishra *et al*.[2] for producing ultra-fine grained (UFG) materials with improved properties. In context of common SPD methods such as high pressure torsion, equal channel angular extrusion and accumulative roll bonding,[3–5] FSP can produce bulk UFG materials in a single pass.

In FSP, a non-consumable rotating tool with a shoulder and pin is traversed along the specific region on a workpiece. Various mechanisms leading to the texture and microstructural evolution has not been clearly understood for this process. Although most of the FSP research has been done on FSP of aluminum alloys, the underlying micro-mechanisms of deformation and restoration is still a mystery. An elementary view point on this subject was presented by McNelley *et al*.,[6] where the authors gave a due emphasis on the recrystallization mechanisms during both FSW and FSP of aluminum alloys. Dynamic recovery along with geometric dynamic recrystallization and particle stimulated nucleation (PSN) was identified as the plausible mechanisms in the stir zone of the FSP in alloys 2219 and 5083. However, these studies do not emphasize on the evolution of texture in detail[7,8] and the mechanisms involved do not lead to any conclusion. The objective of the present work is to improve the understanding on the correlation of crystallographic texture and microstructure in FSP as applicable to aluminum alloys. It is possible that in a process like FSP where the shear directions change in different regions, the localized texture measurements by EBSD do not reveal the overall texture present in the nugget zone. Since the bulk mechanical properties of materials depend on the overall crystallographic texture, it is highly desirable to examine the overall texture of the nugget zone. The present study aims at examining the same.

Materials selected in the current study were two of the heat treatable aluminum alloys used in structural applications, 2024-T3 and 2219-T87 and a strain hardenable alloy 5086-O. Chemical composition of these three alloys is given in Table I. Thickness of the as received 2024 and 5086 plates were 6 mm, whereas 2219 plate thickness was 7.2 mm. Tool material was hot die steel in H-13 hardened condition. Tool shoulder diameter was taken as 26 mm for the alloys 2024 and 2219, whereas a 30 mm shoulder diameter was used for the alloy 5086. Tool pin was that of a cylindrical tapered shape having a right handed thread and pin length of 5.4 mm, with a top to bottom diameter of 6 to 4 mm. The optimized process parameters based on a bottom-up approach developed by authors[9] was used for the FSP of all three alloys. The optimally processed samples were polished using SiC papers of grade P80 to P3000 and then fine polished using alumina suspension having particle size of 0.3 μm. Electropolishing was done on a Struer's LectroPol-5 electro polisher with the standard A2 electrolyte. A voltage of 26V and a polishing time of 25 seconds was used for the polishing of all three alloys. EBSD was performed on ESEM Quanta microscope having tungsten filament as the electron source (Quanta200, FEI make). TSL orientation imaging microscopy software was used for the microstructure analysis of EBSD data. Bulk texture was measured on a Bruker D8 discover X-ray texture goniometer attached with the area detector Vantec 500. Analysis of the bulk texture has been done using Resmet software.

The characterization results presented in this study is based on a systematic approach developed for optimizing the process parameters of all the three alloys, and the optimally processed sample having the highest tensile

NARESH NADAMMAL, Ph.D. Student, and SATISH V. KAILAS, Professor, are with the Department of Mechanical Engineering, Indian Institute of Science, Bangalore 560012, Karnataka, India. Contact e-mail: nareshnn@mecheng.iisc.ernet.in JERZY SZPUNAR, Professor, Canada Research Chair (Tier I) of Advanced Materials for Clean Energy, is with the Department of Mechanical Engineering, University of Saskatchewan, Saskatoon, SK S7N 5A9, Canada. SATYAM SUWAS, Associate Professor, is with the Department of Materials Engineering, Indian Institute of Science, Bangalore, 560012, Karnataka, India.

Manuscript submitted November 13, 2014.
Article published online April 18, 2015

Table I. Elemental Composition of the Alloys

Alloy	Al	Cu	Mg	Mn	Si	Fe	Ti	Cr	Zn
2024	94.8	3.64	1.45	0.45	0.06	—	—	—	0.05
2219	94.23	5.2	0.17	0.17	0.15	—	0.03	—	0.02
5086	95.2	0.02	4.35	0.35	—	0.02		0.05	0.03

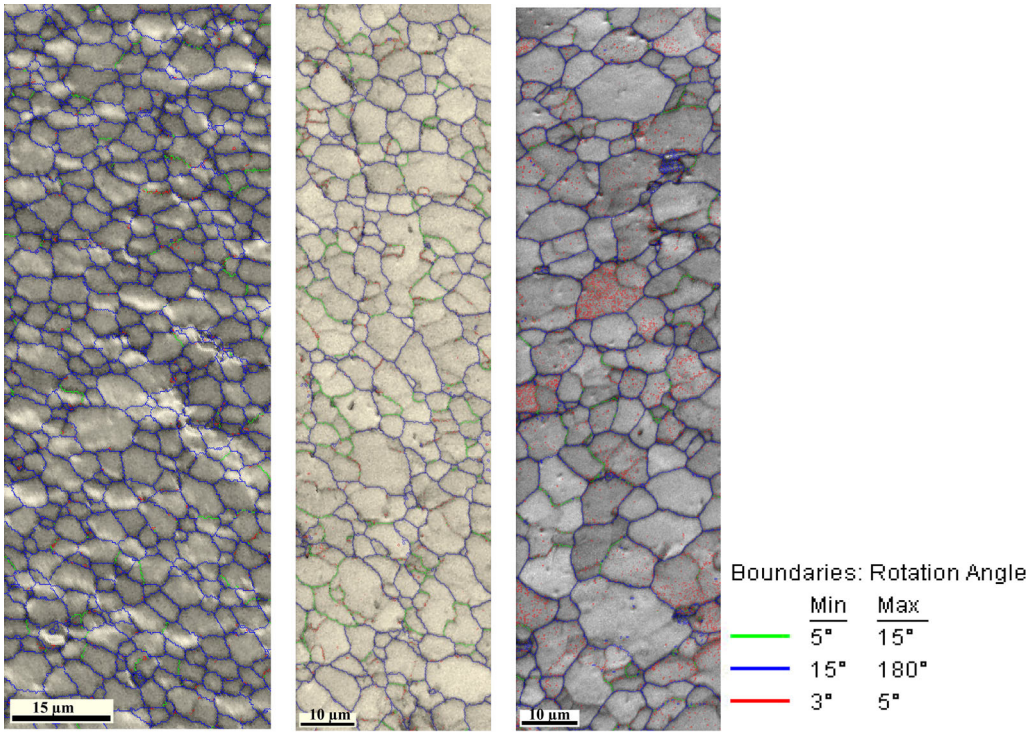

Fig. 1—Image quality map with grain boundary map super imposed for different alloys (*a*) 2024 (*b*) 2219 (*c*) 5086.

Table II. Average Grain Size in the Nugget Zone of FSPed Samples

Alloy	Average Grain Size (μm)
2024-T3	4.2
2219-T87	8
5086-O	10

strength is only considered. Residual stresses measured on the surface of processed samples have depicted similar trends in all the alloys with highly compressive stress values in the nugget zone. These factors indicate that the thermal and thermo-mechanical conditions applied to the materials are almost similar when using an optimum set of process parameters which avoids any discontinuity in the processed volume during FSP.

Figure 1 displays the image quality map super imposed with the grain boundary map obtained from EBSD. Low (3 deg to 5 deg), medium (5 deg to 15 deg), and high angle boundaries (15 deg to 180 deg) are highlighted as red, green, and blue, respectively. Average grain size measured in the nugget zone is given in Table II. It can be observed that under identical processing conditions, alloy 5086 exhibits the highest grain size.

Microstructure evolution confirmed that more equiaxed grains with smaller grain sizes were observed for the alloy 2024, compared to the alloys 2219 and 5086. This might due to the faster aging kinetics observed in the alloy 2024.[10] Temperature rise during FSP could be sufficient for the solutionizing of alloy in mention. For this alloy, FSP which was done at a tool traverse speed of 95 mm/min can be significant for quick heat removal which will allow dissolution and re-precipitation at a faster rate. Cooling rates involved during FSP can be considered as moderate and hence precipitate formation can occur heterogeneously at the grain boundaries.[9] These precipitates can inhibit further grain growth. However, for the heat treatable alloy 2219, aging kinetics is comparatively slower than that of 2024, therefore comparatively larger grain size is observed.[11] In the alloy 5086, other than the matrix Al_6Mn and Al_6Fe particles are generally observed, but the fraction of Fe in the alloy being much lesser Mn, only the effect of Al_6Mn particles needs to be considered. However, volume fraction of these particles will be lesser than the pre-

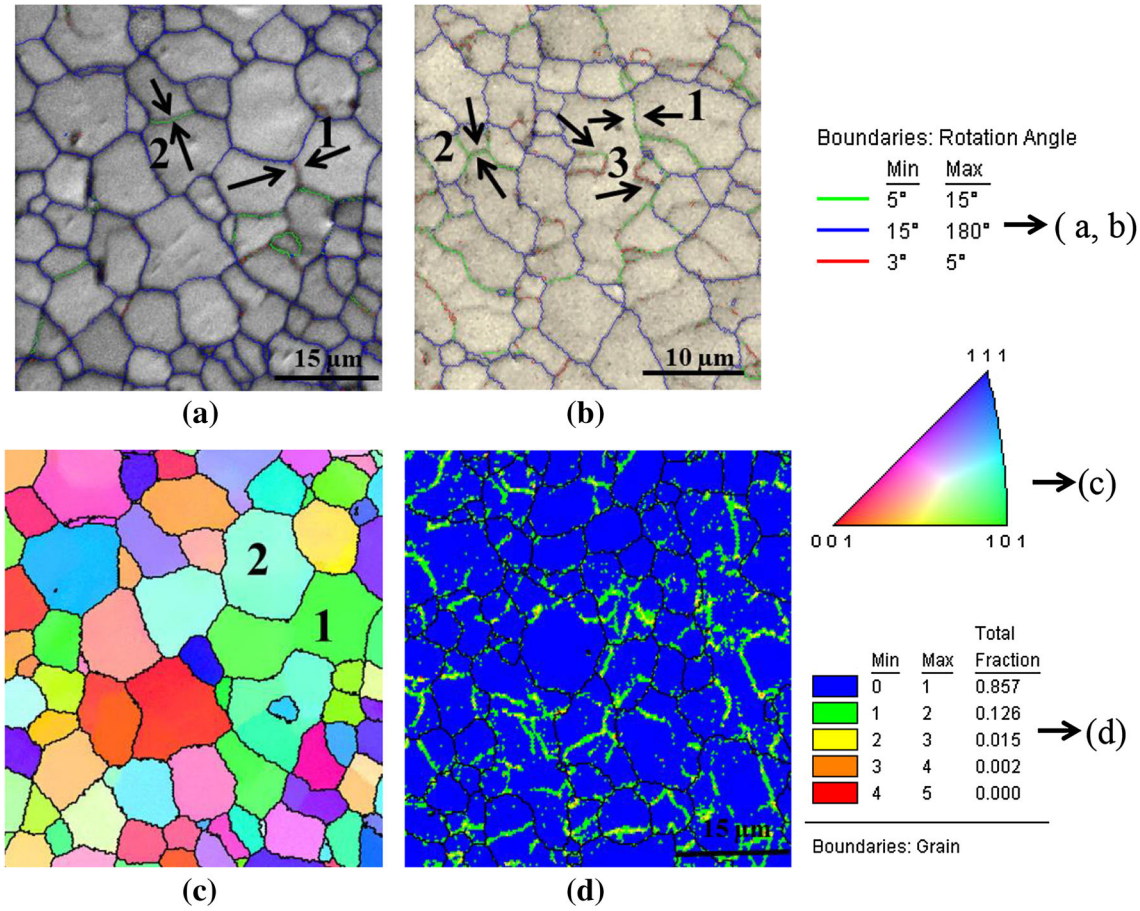

Fig. 2—EBSD maps showing the microstructural evolution in the nugget zone (*a*) and (*b*) image quality (IQ) map with grain boundaries overlapped for 5086 and 2219, respectively, (*c*) inverse pole figure (IPF) map corresponding to the IQ map shown in (a); (*d*) kernel average misorientation (KAM) map for the 5086 alloy. Reference maps for images are shown at the right end. Scale marker for (c) is same as in (a).

cipitates in heat treatable alloys. Grain growth is inhibited only where these particles are present in the matrix. Hence, a higher average grain size is observed for this alloy. Similar results were also observed by Peel *et al.*[12] in their work done exclusively on AA 5083 alloy. Some very fine grains are also observed in the nugget zone for this alloy and this could be due to the particle stimulated nucleation (PSN).

Dynamic recrystallization seems to be responsible for the finer microstructure evolved during FSP. It is therefore worthwhile to discuss the mechanisms of dynamic recrystallization and hence a more detailed information on the features of microstructure evolution can be elucidated from the EBSD analysis results shown in Figure 2. Kernel average misorientation (KAM) map for the alloy 5086 is shown in Figure 2(d). The figure clearly indicates that the misorientations near the grain boundaries are the highest. Similar KAM profile is observed in the case of heat treatable alloys along with comparatively higher misorientations in the grain interiors which may be due to the effect of precipitate particles that are observed in a higher volume fraction. In the case of 2219, as shown in Figure 2(b) bulging at the grain boundary can be observed at the location marked as 3. Such features can be observed in the other regions of microstructure also. These features resemble the nucleation stage during strain-induced boundary migration (SIBM) and thus indicate SIBM as the possible nucleation mechanism in friction stir processed aluminum alloys. SIBM has been reported as the nucleation mechanism in the case of high-temperature deformation of aluminum.[13] A closer evaluation of Figure 2(b) reveals more features confirming SIBM, such as the migrated boundaries in the form of bulges which are further surrounded by low energy dislocation structure in the form of a low-angle boundary.

A significant difference between the microstructures of heat treatable and non-heat treatable alloys are the extent of waviness of grain boundaries. More straight boundaries are observed in alloy 5086 and rather wavy boundaries are observed for the heat treatable alloys. This can arise due to two reasons, the static annealing which can occur during and after FSP and the effect of precipitate particles during microstructural evolution. Faster recrystallization kinetics is observed for Al-Mg alloys compared to other heat treatable aluminum alloys[14] and hence the possibility of static annealing during FSP can be higher for 5086 alloy. PSN can produce a ragged grain boundary structure[15] as shown in Figure 2(b). Large particles capable of becoming nuclei for DRX were observed in the case of heat treatable alloys.[9] These particles were confirmed as

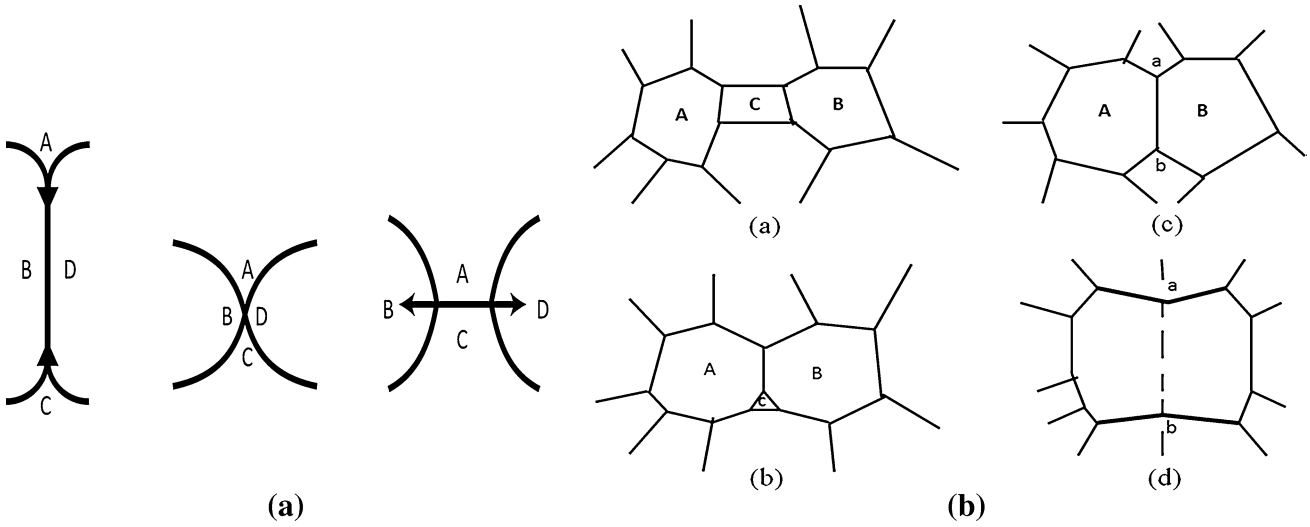

Fig. 3—Schematic representation of two dimensional grain growth mechanisms (*a*) Burke and Turnbull mechanism (*b*) geometrical coalescence.[16,17]

Al_2CuMg and Al_2Cu in case of 2024 and 2219, respectively, from the characterization done using electron probe micro analysis. A more vivid and pronounced bulge formation near to grain boundaries in Figure 2(b) indicates the effect of PSN in addition to SIBM for the heat treatable alloys.

Hence, SIBM and PSN both can simultaneously act as the nucleation mechanisms for DRX in aluminum alloys during FSP. SIBM can be the dominant mechanism for strain hardenable alloys and a minor contribution can also come through the PSN by Al_6Mn particles in the alloy 5086. This was confirmed through the few very fine grains observed in the microstructure of the alloy. Both these mechanisms are equally important in case of heat treatable alloys. As the nucleation mechanisms are explained, next are the grain growth mechanisms. Significant evidence of the normal two-dimensional grain growths was obtained from the obtained IQ map of EBSD scans done on all the alloys. Most important observation was that FSP being a high-temperature deformation process; thermodynamic stability criterions based on energy considerations can play a significant role. This was confirmed through the nugget zone microstructure which was very high in the fraction of grain boundary triple junctions arranged in their stable dihedral angle configuration and larger misorientation gradients present in some grains. Higher misorientations develop in grains due to the fact that a stable end orientation could not be achieved due to the dominance of energy considerations in FSP.

Grain growth in 2D occurs through two major mechanisms known as Burke and Turnbull mechanism[16] and geometrical coalescence proposed by Nielsen[17] as shown schematically in Figures 3(a) and (b), respectively. In Burke and Turnbull mechanism, the criterion is reduction in curvature of grain boundary triple junctions as shown in three sequences in Figure 3(a). Triple junctions form readily at the grain boundaries during high-temperature deformation in FSP with the stable dihedral angle configuration of 120 deg. The process continues until a stable crystallographic orientation develops or the growth gets hindered due to reasons like particle pinning. Such observations were found in the nugget zone of friction stir processed samples in Figure 2(b), marked as regions 1, 2, and 3. These are represented with low and medium angle boundaries that correspond to the microstructural evolution stage of FSP.

Occurrence of some large grains and regions of similarly oriented grains (based on color scheme in an IPF map) is a common feature in the FSP microstructure of all the aluminum alloys studied. Geometrical coalescence can easily occur in such favored situations. Geometrical coalescence occurs as a process by which grains having less than six sides (grain 'C' in Figure 3(b)) lose their sides easily through the formation of grains with much lesser number of sides. During such a process, if the boundary formed between such grains is of a lower energy than the average grain boundary energy (region marked as 1 in Figure 2(a)) then these grains coalesce to form a single grain. Such a grain can be observed left to the grain, which is marked as 1 (same grain is marked as 2 in Figure 2(c) also) in Figure 2(a). Another boundary marked as 2 in Figure 2(a) is between the grains of different orientations (depicted by different color) in the IPF map. Boundary between them is a low angle boundary and these two can coalesce together and form as a single grain.

Bulk crystallographic texture as measured using XRD is shown as (111) pole figures in Figure 4(a) for the three alloys. The volume fractions of major deformation and recrystallization texture components and common fiber textures are shown in Figure 4(b). A key (111) pole figure with shear plane normal and shear direction indicated for FSP specimen geometry is also presented in Figure 4(c), in which the locations of ideal FCC shear texture components are also shown.

Bulk texture measurements reveal weaker texture for all the three alloys studied. Weaker texture intensities develop in FSP due to the deformation at a very high

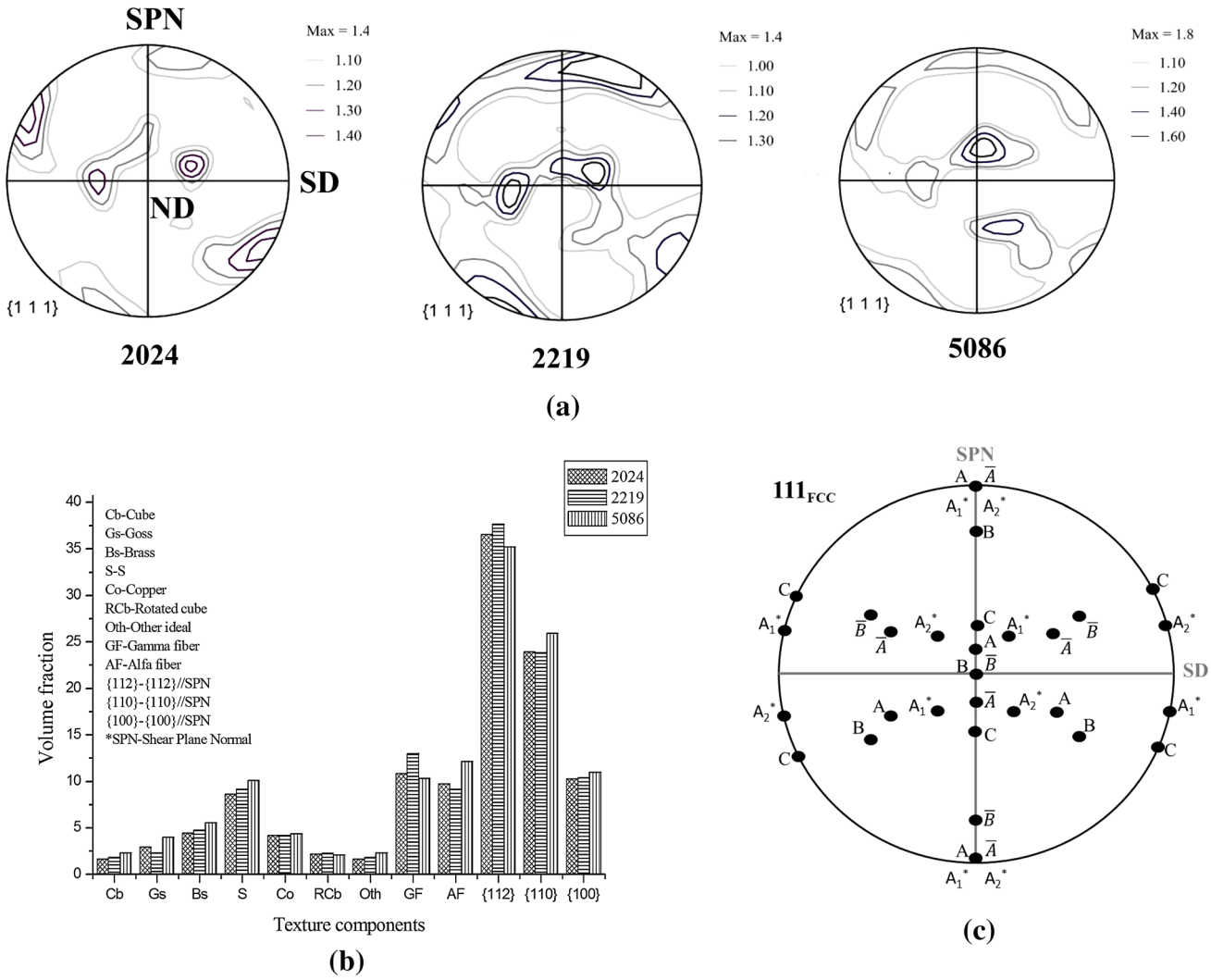

Fig. 4—(*a*) (111) Pole figures representing bulk textures measured from optimum FSP samples of different alloys; shear frame of reference is given for alloy 2024 and similar for other two alloys (SPN-shear plane normal, SD-shear direction, ND-normal direction) (*b*) volume fraction of texture components (*c*) standard (111) pole figure with locations of ideal FCC shear components; A* is identical as $\bar{A}$, B* is identical as $\bar{B}$.

temperature where the equilibrium texture component can be due to the deformation as well as recrystallization. As noticed earlier, the nucleation mechanisms for DRX were identified as SIBM and PSN with their respective dominance in heat treatable and non-heat treatable alloys. Both of these mechanisms are reported to produce significantly weak textures in aluminum alloys.[18]

It is generally assumed that the deformation mode during FSP is predominantly shear. Therefore, the deformation components of texture have been analyzed as that of shear texture. Shear texture components for FCC materials are located and shown given in Figure 4(c). Volume fractions of various texture components in all the three alloys have confirmed the presence of similar components and intensity. The {112} fiber parallel to the shear plane normal was the major component with a volume fraction of 35 to 40 pct for all the alloys. This is the common B/B* component which is indicative of the large shear strain imparted during FSP.[19,20] An equal fraction of this component indicates the occurrence of similar kind of deformation in aluminum alloys irrespective of their response to heat treatment. The (111) pole figure for 5086 shows the presence of C component. For this component, the shear plane normal will be {001} and the shear direction is ⟨110⟩. The occurrence of C component could be due to the annealing phenomenon occurring during FSP. It has been already observed that the static annealing after deformation occurs in the alloy 5086-O. Hence, the occurrence of this component in a relatively larger fraction can be justified in this alloy because {001} is a part of the common recrystallization texture component observed in aluminum alloys.

In summary, optimally friction stir processed aluminum alloys were characterized using EBSD and XRD. Microstructural evolution followed the same pattern in all three alloys irrespective of the different microstructural features of the starting material. SIBM and PSN were the dominant nucleation mechanisms for the DRX in strain hardenable and heat treatable alloys, respectively, which confirms the dependence of

recrystallization behavior on the alloy composition. Grain growth occurs in all the alloys through Burke and Turnbull mechanism and geometrical coalescence. Weak texture was observed in all three alloys and the same is attributed to the observed DRX nucleation mechanisms of SIBM and PSN.

The authors would like to thank Department of Science and Technology (DST), Ministry of Human Resources Development (MHRD), India for financial support and Advanced Facility for Microscopy and Microanalysis (AFMM) at Indian Institute of Science, Bangalore, for providing the facilities. We are also grateful to Government of Canada for selecting first author NN for the Canadian Commonwealth Scholarship Program (CCSP) and allowing usage of the X-ray diffraction facility at Department of Mechanical Engineering, University of Saskatchewan, Saskatoon, Canada.

REFERENCES

1. J.C. Williams and E.A. Starke, Jr: *Acta Mater*., 2003, vol. 51, pp. 5775–99.
2. R.S. Mishra, M.W. Mahoney, S.X. Mcfadden, N.A. Mara, and A.K. Mukherjee: *Scripta Mater*., 2000, vol. 42, pp. 163–68.
3. N.A. Smirnova, V.I. Levit, V.I. Pilyugin, R.I. Kuznetsov, L.S. Davydova, and V.A. Sazonova: *Fiz. Metall. Metalloved*., 1986, vol. 61, pp. 1170–77.
4. V.M. Segal, V.I. Reznikov, A.E. Drobyshevskiy, and V.I. Kopylov: *Russ. Metall*., 1981, vol. 1, pp. 99–105.
5. Y. Saito, H. Utsunomiya, N. Tsuji, and T. Sakai: *Acta Mater*., 1999, vol. 47, pp. 579–83.
6. T.R. McNelley, S. Swaminathan, and JQ Su: *Scripta Mater*., 2008, vol. 58, pp. 349–54.
7. R.W. Fonda and J.F. Bingert: *Scripta Mater*., 2007, vol. 57, pp. 1052–55.
8. R.W. Fonda, J.F. Bingert, and K.J. Colligan: *Scripta Mater*., 2004, vol. 51, pp. 243–48.
9. N. Nadammal, S.V. Kailas, and S. Suwas: *Mater. Des*., 2015, vol. 65, pp. 127–38.
10. Z. Hu, S. Yuan, X. Wang, G. Liu, and Y. Huang: *Mater. Des*., 2011, vol. 32 (10), pp. 5055–60.
11. F. Tariq, N. Naz, and R.A. Baloch: *J. Non-destr. Eval*., 2012, vol. 31 (1), pp. 17–33.
12. M. Peel, A. Steuwer, M. Preuss, and P.J. Withers: *Acta Mater*., 2003, vol. 51 (16), pp. 4791–4801.
13. M.C. Theyssier and J.H. Driver: *Mater. Sci. Eng. A*, 1999, vol. 272 (1), pp. 73–82.
14. C. Genevois, A. Deschamps, and A. Denquin: in *Proceedings of 5th International Symposium on Friction Stir Welding*, Metz, France, September 2004, TWI.
15. N. Hansen and B. Bay: *Acta Metall*., 1981, vol. 29 (1), pp. 65–77.
16. J.E. Burke and D. Turnbull: *Progr. Mater. Phys*., 1952, vol. 3, pp. 220–92.
17. J.P. Nielsen: *ASM Seminar Series*, American Society for Metals, Metals Park, OH, 1966.
18. A. Rollett, F.J. Humphreys, G.S. Rohrer, and M. Hatherly: *Recrystallization and Related Annealing Phenomena*, Elsevier, UK, 2004.
19. R.W. Fonda and K.E. Knipling: *Sci. Technol. Weld*., 2011, vol. 16 (4), pp. 288–94.
20. K.S. Suresh, N. Kumar, R.S. Mishra, and S. Suwas: *Mater. Sci. Forum*, 2013, vol. 753, pp. 247–50.